Biochemical and Biophysical Research Communications 510 (2019) 72–77

Contents lists available at ScienceDirect

Biochemical and Biophysical Research Communications

journal homepage: www.elsevier.com/locate/ybbrc

Fibrillar force generation by fibroblasts depends on formin

Mohamad Eftekharjoo [a], Dakota Palmer [b], Breanna McCoy [c], Venkat Maruthamuthu [a, *]

[a] Department of Mechanical and Aerospace Engineering, Old Dominion University, Norfolk, VA, 23529, USA
[b] Department of Biological Sciences and Old Dominion University, Norfolk, VA, 23529, USA
[c] Department of Engineering Technology, Old Dominion University, Norfolk, VA, 23529, USA

ARTICLE INFO

Article history:
Received 24 December 2018
Accepted 7 January 2019
Available online 17 January 2019

Keywords:
Extra-cellular matrix
Traction force
Micropatterning
Actin nucleation
Mechanobiology
Fibrosis

ABSTRACT

Fibroblasts in the extra-cellular matrix (ECM) often adopt a predominantly one-dimensional fibrillar geometry by virtue of their adhesion to the fibrils in the ECM. How much forces such fibrillar fibroblasts exert and how they respond to the extended stiffness of their micro-environment comprising of other ECM components and cells are not clear. We use fibroblasts adherent on fibronectin lines micropatterned onto soft polyacrylamide gels as an *in vitro* experimental model that maintains fibrillar cell morphology while still letting the cell mechanically interact with a continuous micro-environment of specified stiffness. We find that the exerted traction, quantified as the strain energy or the maximum exerted traction stress, is not a function of cell length. Both the strain energy and the maximum traction stress exerted by fibrillar cells are similar for low (13 kPa) or high (45 kPa) micro-environmental stiffness. Furthermore, we find that fibrillar fibroblasts exhibit prominent linear actin structures. Accordingly, inhibition of the formin family of nucleators strongly decreases the exerted traction forces. Interestingly, fibrillar cell migration is, however, not affected under formin inhibition. Our results suggest that fibrillar cell migration in such soft microenvironments is not dependent on high cellular force exertion in the absence of other topological constraints.

1. Introduction

Physical cues fundamentally influence multiple aspects of cell function including survival, migration, proliferation and differentiation [1]. Among physical cues, cell geometry is a key factor that dictates how cells interact with their micro-environment, mainly by its influence on forces generated and transmitted by the cells themselves [2,3]. Cells embedded in three-dimensional (3D) extracellular matrix (ECM) microenvironments, such as fibroblasts, encounter ECM of complex topology [4]. It has been demonstrated that reductionist one-dimensional (1D) fibrillar microenvironments capture key aspects of 3D matrices wherein fibroblasts are often adherent along fibrils in the matrix [5]. Forces generated by cells adherent on 1D fibrils and aligned matrices can be transmitted over long distances and effect changes in the microenvironment that includes other cells [6]. Previous studies have elucidated how fibrillar cell geometry can lead to altered migration rates, compared to a two-dimensional (2D) context [7]. However, despite recent advances [8], the factors that influence force exertion by fibrillar cells have been largely unclear.

Recent approaches with micro-patterned lines and individual suspended fibrils have provided important insights into fibrillar cell migration [9,10]. However, even when fibroblasts are predominantly constrained in a 1D geometry (adherent on fibrils), they interact with an extended microenvironment consisting of other entangled fibrils, other ECM constituents and cells. While cells in 2D respond to altered stiffness by transmitting altered traction forces [11], it is unclear if cells constrained in 1D geometries can sense surrounding micro-environmental stiffness similarly and modulate transmitted forces [12]. The micro-environmental stiffness encountered by fibroblasts changes during progression of disease states like fibrosis [13]. Thus, it is important to ascertain whether such stiffness cues impact force generation by fibroblasts, which may in turn further modify micro-environmental stiffness in a positive feedback loop.

Previous reports have proposed distinct roles for actin

Abbreviations: ECM, extra-cellular matrix; 1D, one-dimensional; 2D, two-dimensional; 3D, three-dimensional; PAA, polyacrylamide; EDC, 1-ethyl-3-(3-dimethylaminopropyl) carbodiimide hydrochloride; sulfo-NHS, N-hydroxysulfosuccinimide.

* Corresponding author. Mechanical & Aerospace Engineering, 238e Kaufman, 1, Old Dominion University, Norfolk, VA, 23529, USA.
E-mail address: vmarutha@odu.edu (V. Maruthamuthu).

https://doi.org/10.1016/j.bbrc.2019.01.035
0006-291X/

nucleators in fibrillar cell migration [14], but their contribution to fibrillar force generation has not been directly tested. In particular, formin nucleators give rise to prominent linear actin structures in cells [15], but their role in enabling fibrillar cell force generation is unclear. In this paper, we introduce an *in vitro* experimental model that employs micropatterning on soft substrates to quantify force exertion by fibroblasts in a fibrillar (1D) geometry and test its dependence on microenvironmental stiffness and actin nucleation by formin. We also assess whether fibrillar cell migration speeds relate to the level of fibrillar force exerted by fibroblasts.

2. Materials and methods

2.1. Cell culture

NIH 3T3 cells were cultured in Dulbecco's modified Eagle's medium (Corning Inc., Corning NY) supplemented with L-glutamine, sodium pyruvate, 1% Penicillin/streptomycin, and 10% fetal bovine serum (Corning Inc., Corning NY) at 37 °C, under 5% CO_2. For plating micro-patterned polyacrylamide (PAA) hydrogels, about 10^5 cells were plated in 35-mm culture dishes with a micro-patterned hydrogel-coated coverslip and the medium was replaced within 0.5 h after plating.

2.2. Preparation and micropatterning of polyacrylamide hydrogel substrates

PAA gels were made with acrylamide to bisacrylamide ratios of 7.5%:0.1% and 12%:0.1% to yield gels of Young's moduli 13 ± 1 and 45 ± 4 kPa, respectively. The stiffness of the gels were characterized with a Bohlin Gemini parallel plate rheometer (Malvern Instruments, Worcestershire, UK). The gels were doped with red fluorescent beads of diameter of 0.44 μm (Spherotech Inc., Lake Forest, IL) to act as fiducial markers. Micropatterning of the PAA gels was performed as follows [2]: a quartz photomask coated with chrome except for clear lines of 1.5 μm width (Toppan, Round Rock, TX) was cleaned with isopropanol and then wiped with toluene. Then, ~100 μL of an acrylamide/bisacrylamide polymerizing mixture [16–18] was placed on the chrome side of the photomask and sandwiched with a 22×22 mm^2 glass coverslip (Corning Inc., Corning NY) that had been pre-activated by treating with 2% 3-aminopropyltrimethyoxysilane and 1% glutaraldehyde. After PAA gel polymerization, the gel on the mask was exposed to deep UV light (through the mask) for 2.5 min. The PAA gels were then incubated with an aqueous solution with 10 mg/ml each of EDC (1-ethyl-3-(3-dimethylaminopropyl) carbodiimide hydrochloride) and sulfo-NHS (N-hydroxysulfosuccinimide) for 25 min at room temperature. This was followed by incubation with 0.01 mg/ml of fibronectin (Millipore Sigma, Burlington, MA) in 100 mM sodium biocarbonate, pH 8.5 for 30 min. After a few washes with PBS, cells were plated on the PAA gels and imaged about 16 h later.

2.3. Live cell imaging and immunofluorescence

Live and fixed cells were imaged using a Leica DMi8 epifluorescence microscope (Leica Microsystems, Buffalo Grove, IL)

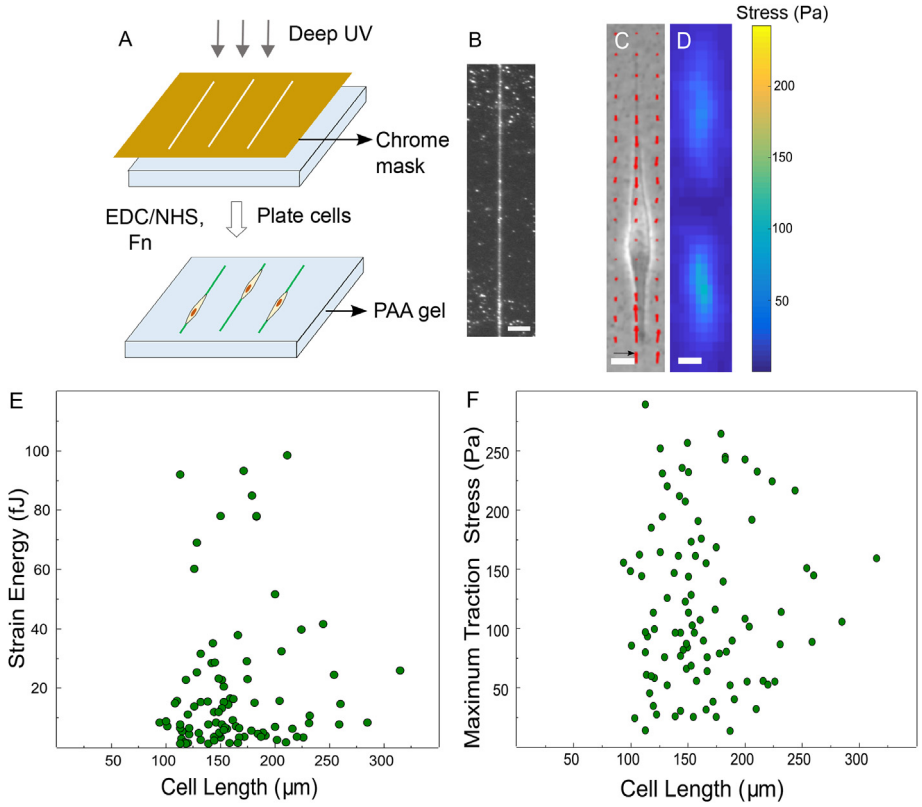

Fig. 1. Fibrillar force exertion is not correlated with cell length. (A) Schematic depiction of the method used to micro-pattern 1.5 μm fibronectin lines on a polyacrylamide (PAA) gel using deep UV illumination of the PAA gel through a chrome-coated quartz photomask, followed by incubation with EDC/sulfo-NHS and fibronectin (Fn). The plated cells adhere to the fibronectin lines and adopt a fibrillar morphology. (B) Fluorescence image of the micropatterned line as revealed by fibronectin doped with fluorescent fibrinogen. (C) Phase image of an NIH 3T3 cell on a 1.5 μm fibronectin line on a 45 kPa PAA gel superimposed with traction stress vectors (red). Scale bar for traction vectors (black arrow) is 100 Pa. (D) Heat map representation of the traction stress exerted. Traction stress heat map color scale is shown on the right. Scale bar in (B–D) is 20 μm. (E) Scatter plot of the strain energy (in fJ) associated with traction force exertion versus cell length (in μm), data from 97 cells. (F) Scatter plot of the maximum traction stress exerted (in Pa) versus cell length (in μm). (For interpretation of the references to color in this figure legend, the reader is referred to the Web version of this article.)

equipped with a 10 × 0.3 NA objective and a Clara cooled CCD camera (Andor Technology, Belfast, UK). An airstream incubator (Nevtek, Williamsville, VA) was used to maintain the temperature at 37 °C during time lapse imaging of live cells. Cells were fixed with 4% paraformaldehyde (Electron Microscopy Sciences, Hatfield, PA) with 1.5% Bovine Serum Albumin and 0.5% Triton. Alexa-488 conjugated phalloidin was from Thermo Fisher Scientific, Waltham, MA. To quantify cell migration speeds, time lapse images of 3T3 cells (on patterned lines on the PAA gel) were acquired every 10 min over a duration of 2 h. Using ImageJ, the cells were manually tracked to locate their position every 10 min. The average cell speed was the sum of the magnitudes of cell displacement every 10 min over 2 h, divided by the total time (2 h).

2.4. Traction force microscopy

First, fibrillar cell phase images and bead fluorescence images, as well as bead fluorescence images after cell detachment (using 10% sodium dodecyl sulfate) were obtained. After image alignment using ImageJ [19], the displacement field was computed using MATLAB (MathWorks, Natick, MA), with code available at http://www.oceanwave.jp/softwares/mpiv/. Traction forces were then reconstructed using regularized Fourier transform traction cytometry which employs the Boussinesq solution [20–24]. The traction exerted was characterized using two metrics: (i) the strain energy stored in the substrate given by $\frac{1}{2}\sum \boldsymbol{T}_i.\boldsymbol{u}_i$ where $\boldsymbol{T}_i$ and $\boldsymbol{u}_i$ are the traction force and displacement vectors at position i, respectively and (ii) the maximum traction stress $\boldsymbol{T}_{max}$, which is the maximum of the magnitudes of all traction stress vectors $\boldsymbol{T}_i$ associated with a given cell.

2.5. Pharmacological inhibition

Pan-formin inhibitor SMIFH2 was from Millipore Sigma, Burlington, MA. NIH 3T3 already plated overnight on fibillar micropatterns were treated with 20 μM SMIFH2 for 4 h prior to live cell imaging.

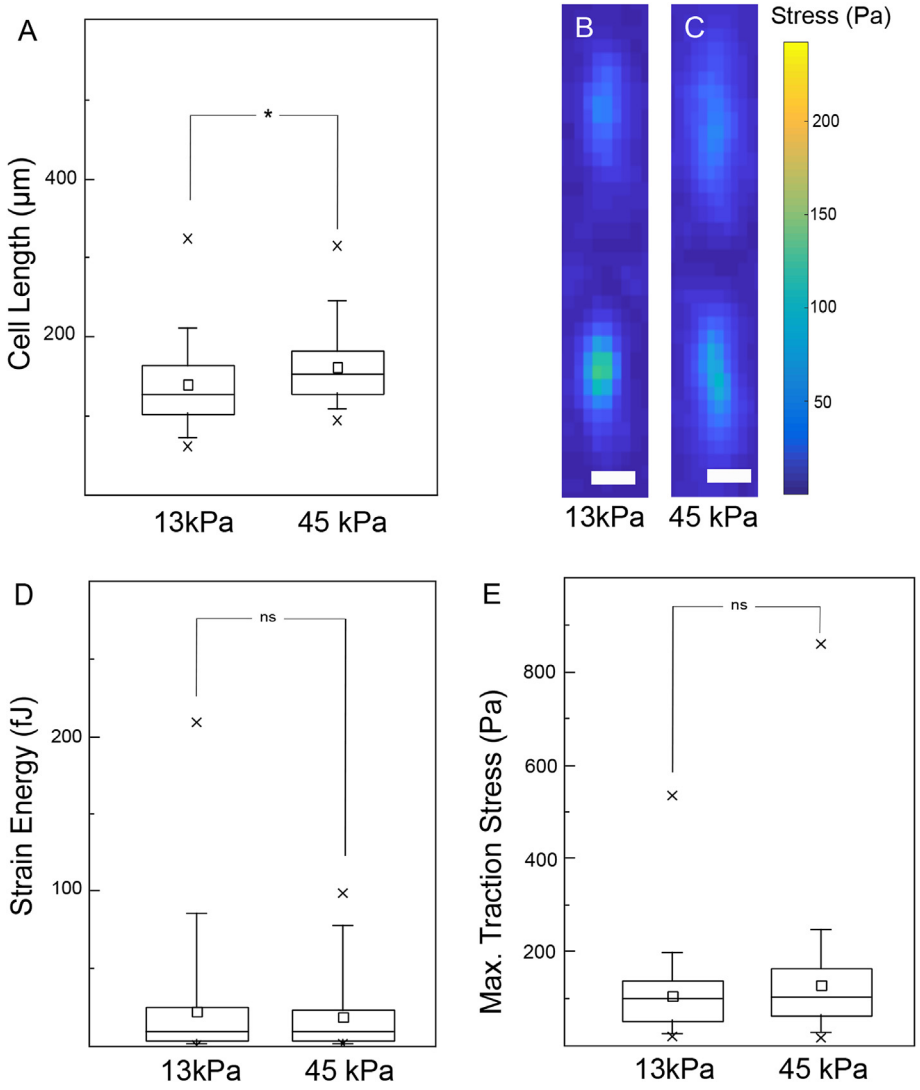

Fig. 2. Fibrillar force exertion is not sensitive to substrate stiffness. (A) Box plot comparing the fibrillar cell length on fibronectin lines on 13 kPa (83 cells) and 45 kPa (97 cells) PAA substrates. (B–C) Heat map representation of the traction stress exerted for substrate Young's moduli of 13 kPa (B) and 45 kPa (C). The scale bars for distance is 20 μm. Traction stress heat map color scale is shown on the right. (D, E) Box plots comparing the strain energy (D) and the maximum traction stress (E) exerted by cells adherent on fibronectin lines on substrates of Young's moduli 13 kPa and 45 kPa. In the box plots, the small square represents the mean, the horizontal line represents the median, cross (x) represents minimum or maximum value, lower and upper sides of the large box represent the 25 and 75 percentile values and whiskers represent the 5 and 95 percentile values. (For interpretation of the references to color in this figure legend, the reader is referred to the Web version of this article.)

2.6. Statistical analysis

For statistical comparisons, two-tailed student's t-test was used with $p < 0.01$ considered significant ('*' = $p < 0.01$ and '**' = $p < 0.001$).

3. Results and discussion

We wanted to employ an experimental model that would restrict fibroblast adhesion to 1D but simultaneously enable them to mechanically interact with a soft micro-environment of defined stiffness. It has been previously shown [5] than lines more than a couple of μm in width increasingly mimic 2D cell morphologies and that a line width of 1.5 μm enables fibrillar cell morphology. We therefore micro-patterned 1.5 μm-wide lines of fibronectin on PAA gels of defined stiffness (Young's modulus 45 kPa), plated NIH 3T3 fibroblast on them and allowed the cells to adhere to the lines overnight (Fig. 1A and B). NIH 3T3 cells adhered only to the fibronectin lines and adopted a 1D fibrillar morphology (Fig. 1C), consistent with previous reports [5,14,25]. We then determined the traction forces exerted by the single cells adherent on single fibronectin lines on the PAA gel. Fig. 1C shows the traction stress vectors overlaid on a fibrillar cell image and Fig. 1D shows the heatmap representation of the traction stress field. The traction stress is mainly localized at the two ends of the cell, consistent with recent reports [12,25,26]. Fig. 1E and F shows how two metrics associated with the exerted traction, strain energy and maximum traction stress varies with cell length. It is evident that there is no clear correlation between either traction metric and the cell length, in contrast to what has been observed in wider lines [25] and 2D [2,3].

In order to assess the role of micro-environmental stiffness in fibrillar cell force exertion, we micropatterned fibronectin lines on PAA gels of stiffness 13 and 45 kPa, within a range of stiffness at which the traction force for 3T3 cells varies with stiffness in 2D [2,27]. The difference in cell lengths corresponding to these substrate stiffnesses was statistically significant but <15% (Fig. 2A). As shown by the traction maps in Fig. 2B and C, the traction stress exerted by fibrillar 3T3 cells was prominently localized at either cell end for both stiffnesses. Importantly, both the strain energy

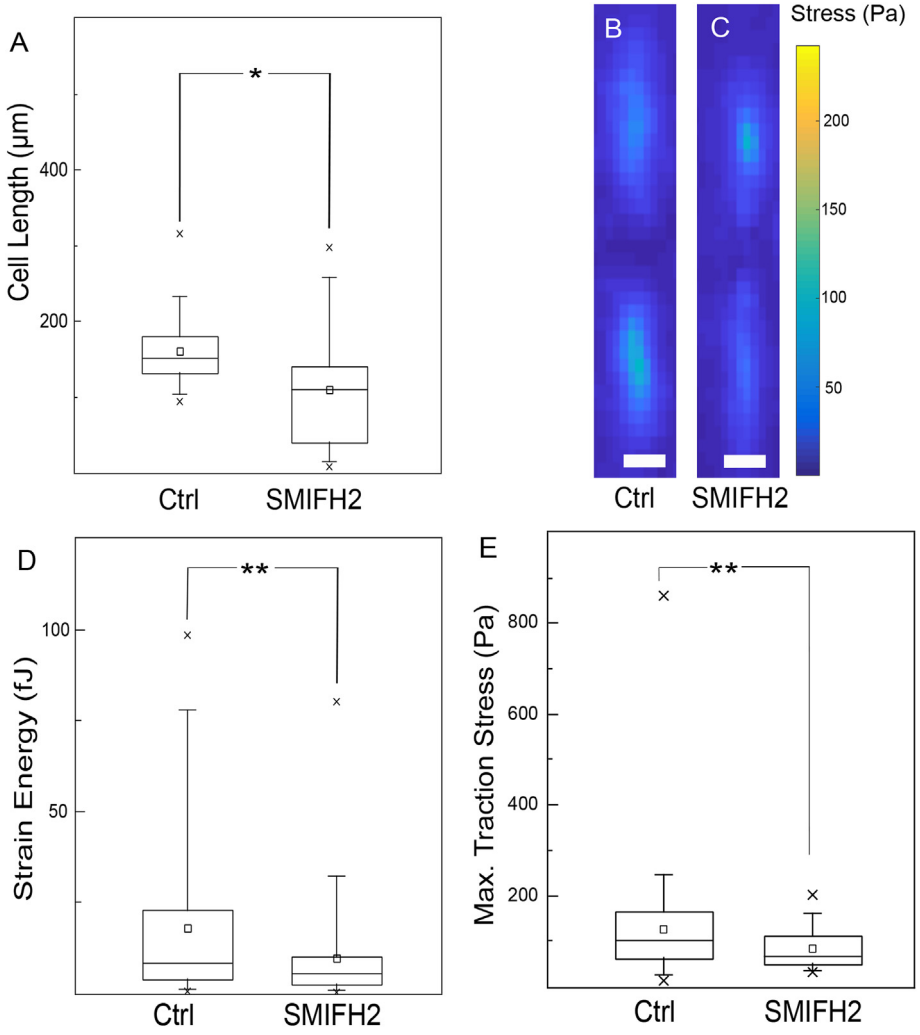

Fig. 3. Effect of formin inhibition on fibrillar force exertion. (A) Box plot comparing the fibrillar cell length on fibronectin lines for control (97 cells) and 20 μM SMIFH2-treated (57 cells) cells on 45 kPa PAA substrates. (B–C) Heat map representation of the traction stress exerted by control and SMIFH2-treated cells. The scale bars for distance is 20 μm. Traction stress heat map color scale is shown on the right. (D, E) Box plots comparing the strain energy (D) and the maximum traction stress (E) exerted by control and SMIFH2-treated cells. In the box plots, the small square represents the mean, the horizontal line represents the median, cross (x) represents minimum or maximum value, lower and upper sides of the large box represent the 25 and 75 percentile values and whiskers represent the 5 and 95 percentile values. (For interpretation of the references to color in this figure legend, the reader is referred to the Web version of this article.)

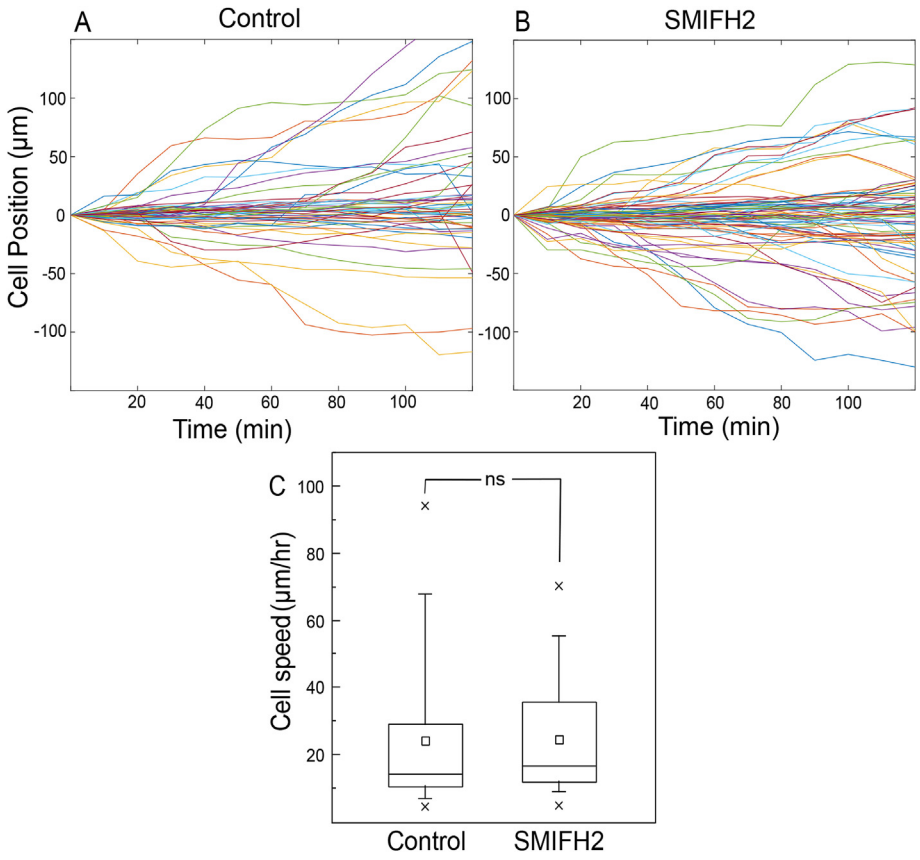

Fig. 4. Fibrillar cell migration speed is not affected by formin inhibition. (A, B) Cell position is plotted as a function of time over 2 h for (A) control (56 cells) and (B) SMIFH2 treated (77 cells) 3T3 cells. Cells were on 1.5 μm fibronectin lines on 45 kPa PAA gels for both cases. (C) Box plots comparing the fibrillar cell migration speed for control versus SMIFH2-treated cells. In the box plots, the small square represents the mean, the horizontal line represents the median, cross (x) represents minimum or maximum value, lower and upper sides of the large box represent the 25 and 75 percentile values and whiskers represent the 5 and 95 percentile values.

(Fig. 2D) and the maximum traction stress (Fig. 2E) of the fibrillar cells did not change significantly with stiffness ($p = 0.39$ and 0.11, respectively). This implies that fibrillar cells exert forces in a manner that is not as strongly sensitive to the microenvironmental stiffness as for 2D [2]. However, as the difference in cell lengths for these different stiffnesses is not large, one can expect the strain energy to not be affected by much if geometry (which translates to cell length here) is indeed a determinant of strain energy [2].

We then wanted to determine as to what factors influence the level of forces exerted by fibroblasts in a fibrillar geometry. Immunofluorescence staining of the actin cytoskeleton showed that the cells displayed prominent linear actin bundles along the length of the cell, anchored at either end of the cell (Fig. S1A). We therefore tested if inhibiting formin, which is a family of linear actin nucleators, would impact the actin cytoskeleton and thereby possibly affect cell force exertion. Accordingly, treatment of fibrillar cells with 20 μM SMIFH2, a pan-formin inhibitor, decreased actin localization to the ends of the cell (Figs. S1B and C). Formin inhibition also reduced the fibrillar cell length by 25% (Fig. 3A). Importantly, traction force measurements showed that formin inhibition reduced the strain energy and the maximum exerted traction stress by 46 and 35%, respectively (Fig. 3B–E) - effects similar to that found in 2D [28].

Finally, we wanted to assess whether reducing the level of traction forces exerted by the cells adversely impacted fibrillar cell migration. We therefore measured the fibrillar cell migration speeds of control cells as well as those treated with the formin inhibitor SMIFH2 (Fig. 4A and B). Contrary to what was found in suspended fibers [14], formin inhibition did not significantly alter the average fibrillar cell migration speed ($p = 0.89$, Fig. 4C). Thus, fibrillar cell migration speed was not correlated to the level of fibrillar force exertion. This result is similar to what was obtained for untreated epithelial cells on wider lines, albeit specifically for only the more elongated cells [25]. The difference in results between our experimental model and that from studies using suspended fibrils may be due to the following reasons [10,14]: our model captures the overall micro-environmental stiffness of tissues, which is in the kPa range. Suspended fibers (made of polymers such as polystyrene) have stiffness in the GPa range [10], similar to that of individual collagen fibrils [29]. In fact, average cell migration rates were about a factor of two to three lower in our system compared to suspended fibrils [14] or micro-patterned lines on glass [5]. Fibrillar cells *in vivo* may be expected to mechanically interact with both the local stiff fibril as well as the softer extended micro-environment. Greater knowledge of forces exerted by cells in fibrillar contexts [30] and their reciprocal relationship with micro-environmental stiffness can be expected to continue to advance our understanding of disease states such as cancer and fibrosis.

Acknowledgments

We thank Margaret Gardel for generously allowing use of the rheometer. We thank Benedikt Sabass and Ulrich Schwarz for the force reconstruction scripts.

Appendix A. Supplementary data

Supplementary data to this article can be found online at https://doi.org/10.1016/j.bbrc.2019.01.035.

Transparency document

Transparency document related to this article can be found online at https://doi.org/10.1016/j.bbrc.2019.01.035.

Funding

This work was supported by the Thomas F. and Kate Miller Jeffress Memorial Trust. The funding source had no role in study design; in the collection, analysis and interpretation of data; in the writing of the report; or in the decision to submit the article for publication.

References

[1] V. Vogel, M. Sheetz, Local force and geometry sensing regulate cell functions, Nat. Rev. Mol. Cell Biol. 7 (4) (2006) 265–275.
[2] P.W. Oakes, et al., Geometry regulates traction stresses in adherent cells, Biophys. J. 107 (4) (2014) 825–833.
[3] S.J. Han, et al., Decoupling substrate stiffness, spread area, and micropost density: a close spatial relationship between traction forces and focal adhesions, Biophys. J. 103 (4) (2012) 640–648.
[4] A.D. Doyle, K.M. Yamada, Mechanosensing via cell-matrix adhesions in 3D microenvironments, Exp. Cell Res. 343 (1) (2016) 60–66.
[5] A.D. Doyle, et al., One-dimensional topography underlies three-dimensional fibrillar cell migration, J. Cell Biol. 184 (4) (2009) 481–490.
[6] N. Gjorevski, et al., Dynamic tensile forces drive collective cell migration through three-dimensional extracellular matrices, Sci. Rep. 5 (2015) 11458.
[7] A.D. Doyle, et al., Dimensions in cell migration, Curr. Opin. Cell Biol. 25 (5) (2013) 642–649.
[8] K. Sheets, et al., Nanonet force microscopy for measuring cell forces, Biophys. J. 111 (1) (2016) 197–207.
[9] A.D. Doyle, et al., Micro-environmental control of cell migration–myosin IIA is required for efficient migration in fibrillar environments through control of cell adhesion dynamics, J. Cell Sci. 125 (Pt 9) (2012) 2244–2256.
[10] A. Hall, et al., Nanonet force microscopy for measuring forces in single smooth muscle cells of the human aorta, Mol. Biol. Cell 28 (14) (2017) 1894–1900.
[11] J.P. Califano, C.A. Reinhart-King, Substrate stiffness and cell area predict cellular traction stresses in single cells and cells in contact, Cell. Mol. Bioeng. 3 (1) (2010) 68–75.
[12] S.J. Han, et al., Spatial and temporal coordination of traction forces in one-dimensional cell migration, Cell Adhes. Migrat. 10 (5) (2016) 529–539.
[13] R.G. Wells, Tissue mechanics and fibrosis, Biochim. Biophys. Acta 1832 (7) (2013) 884–890.
[14] C. Guetta-Terrier, et al., Protrusive waves guide 3D cell migration along nanofibers, J. Cell Biol. 211 (3) (2015) 683–701.
[15] S.H. Zigmond, Formin-induced nucleation of actin filaments, Curr. Opin. Cell Biol. 16 (1) (2004) 99–105.
[16] T. Yeung, et al., Effects of substrate stiffness on cell morphology, cytoskeletal structure, and adhesion, Cytoskeleton 60 (1) (2005) 24–34.
[17] V. Maruthamuthu, et al., Cell-ECM traction force modulates endogenous tension at cell-cell contacts, Proc. Natl. Acad. Sci. U. S. A. 108 (12) (2011) 4708–4713.
[18] V. Maruthamuthu, M.L. Gardel, Protrusive activity guides changes in cell-cell tension during epithelial cell scattering, Biophys. J. 107 (3) (2014) 555–563.
[19] J.L. Martiel, et al., Measurement of cell traction forces with Image, J. Meth. Cell Biol. 125 (2015) 269–287.
[20] J.P. Butler, et al., Traction fields, moments, and strain energy that cells exert on their surroundings, Am. J. Physiol. Cell Physiol. 282 (3) (2002) C595–C605.
[21] S.V. Plotnikov, et al., High-resolution traction force microscopy, Methods Cell Biol. 123 (2014) 367–394.
[22] B. Sabass, et al., High resolution traction force microscopy based on experimental and computational advances, Biophys. J. 94 (1) (2008) 207–220.
[23] U.S. Schwarz, et al., Calculation of forces at focal adhesions from elastic substrate data: the effect of localized force and the need for regularization, Biophys. J. 83 (3) (2002) 1380–1394.
[24] I. Muhamed, F. Chowdhury, V. Maruthamuthu, Biophysical tools to study cellular mechanotransduction, Bioengineering 4 (1) (2017) 12.
[25] A. Leal-Egana, et al., The size-speed-force relationship governs migratory cell response to tumorigenic factors, Mol. Biol. Cell 28 (12) (2017) 1612–1621.
[26] A. Ray, et al., Anisotropic forces from spatially constrained focal adhesions mediate contact guidance directed cell migration, Nat. Commun. 8 (2017) 14923.
[27] C.M. Lo, H.B. Wang, M. Dembo, Y.L. Wang, Cell movement is guided by the rigidity of the substrate, Biophys. J. 79 (2000) 144–152.
[28] P.W. Oakes, et al., Tension is required but not sufficient for focal adhesion maturation without a stress fiber template, J. Cell Biol. 196 (3) (2012) 363–374.
[29] M.P. Wenger, et al., Mechanical properties of collagen fibrils, Biophys. J. 93 (4) (2007) 1255–1263.
[30] A. Mukherjee, et al., Design of fiber networks for studying metastatic invasion, in: C. Dong, N. Zahir, K. Konstantopoulos (Eds.), Biomechanics in Oncology, Springer International Publishing, Cham, 2018, pp. 289–318.